Pool Fire-Ventilation Crossflow Experiments in a Simulated Aircraft Cabin Interior

C. P. Bankston* and L. H. Back†
Jet Propulsion Laboratory, California Institute of Technology, Pasadena, California

An experimental facility has been built and instrumented at the Jet Propulsion Laboratory to study pool fire dynamics and flame spread in a 1/3-scale simulated aircraft cabin interior. In this paper, the results of pool fire-ventilation crossflow experiments are reported utilizing a "channel" pool fire subjected to crossflow velocities that replicate possible flow conditions in a postcrash wide-body aircraft. Measurements made include detailed gas-phase temperatures, fuel evaporation rate, radiative and total heat fluxes, oxygen concentrations, and flowfield characteristics. The nominal crossflow velocity was varied from 0.24-0.8 m/s and results show that the energy release rates and combustion efficiency decrease with decreasing flow velocity. The crossflow velocity had a strong effect on visible flame geometry, tending to tilt the flame over sharply. However, a reverse-flow ceiling jet of hot gases was also present in all tests, extending far upstream of the fire. That is, despite the appearance of the visible flame, the vertical momentum of the plume was strong enough to establish the reverse-flow layer, thus spreading smoke and toxic gases upstream against a significant ventilating flow. These data provide new details on fire and flow interactions in ventilated, tunnel-like geometries. The observed general flow characteristics have also been observed in mine tunnel fires and thus the information presented has application in the evaluation of hazards from fires in aircraft fuselage interiors, mine tunnels, and building corridors.

Nomenclature

A = cross-sectional area of test section, 1.16 m^2
b = fuel pan width, 0.30 m
c = specific heat of combustion gases, J/g·K
$\mathfrak{F}$ = fire-crossflow parameter, $2gH\dot{Q}/\rho_g cT_s A\bar{u}^3$
g = gravitational acceleration, 9.8 m/s^2
h_i = reverse-flow layer depth at the ith flow direction probe location in the downstream (x) direction, cm
h_s = smoke layer depth at the first flow direction probe (x = 1.68 m) just downstream of the test section inlet, cm
H = test section vertical height, 0.76 m
m_f = fuel mass loss (evaporation) rate, g/s
$\dot{q}_{r_n}$ = radiative heat flux at the test section ceiling at the nth radiometer location in the downstream (x) direction, W/cm^2
$\dot{q}_{t_n}$ = total heat flux at the test section ceiling at the nth calorimeter location in the downstream (x) direction W/cm^2
$\dot{Q}$ = energy release rate of the pool fire, kW
$\dot{Q}_a$ = available chemical energy release rate calculated from the product of fuel evaporation rate and heat of combustion, kW
$\dot{Q}_e$ = energy required to evaporate the fuel calculated from the product of fuel evaporation rate and heat of vaporization, kW
$\dot{Q}_s$ = convective energy transport through the exhaust stack, kW
$\dot{Q}_w$ = energy transferred to the fuel pan cooling water, kW
T_a = ventilating air ambient temperature, K
T_m = peak measured gas-phase temperature in the test section, K
T_s = mixed mean temperature of exhaust gases, K
u = local gas flow velocity in the x direction, m/s
$\bar{u}$ = nominal gas flow velocity in the x direction just upstream of the fuel pan, m/s
W = test section span width, 1.52 m
x = coordinate in the ventilation flow direction, m
y = coordinate in the vertical direction, m
z = coordinate in the spanwise direction (see Fig.7), m
β = coefficient of volume expansion, K^{-1}
η = combustion efficiency ($\dot{Q}/\dot{Q}_a$)
θ = $T_s - T_a$, K
ρ_g = density of incoming ventilation air, g/cm^3
ρ_s = smoke particulate density in the exhaust stack flow, mass of particulates per unit volume of gas, g/cm^3

Received Sept. 17, 1984; revision received June 5, 1985.

*Member Technical Staff, Mechanical and Chemical Systems Division. Member AIAA.

†Technical Group Supervisor, Mechanical and Chemical Systems Divison. Associate Fellow AIAA.

Introduction

THE role of fire spread in aircraft fire safety is very important since it determines the time in which a fire grows to dangerous proportions in the cabin or other compartments. In the postcrash fire scenario, there is a need for an understanding of the interaction of the fire plume with crossflow ventilation and the flame spread characteristics of aircraft interior materials. However, the mechanisms and processes that control fire dynamics, ignition, and flame spread rates are extremely complex and depend on a variety of physical and chemical parameters. In order to identify the controlling parameters, experimental data are needed for an adequate understanding of observed fire spread phenomena.

The postcrash fuel fire has been studied in full-scale experiments[1-4] at the Federal Aviation Administration Technical Center (FAATC) utilizing a C-133 aircraft fuselage to simulate a wide-body commercial transport aircraft cabin. These experiments have been directed toward evaluating hazards associated with penetration of a large (2.5×3.0 m) fuel pool fire through an opening into the cabin. State-of-the-art and advanced interior panel and seating materials are tested and evaluated for their possible contributions to or prevention of fire propagation and accompanying fire hazards. These data are also compared with the results from standard small-scale tests in order to evaluate the ability of the small-scale tests to predict full-scale results.[4,5] An analysis of these tests by Quintiere and Tanaka[6] has emphasized the importance of wind in predicting relative cabin hazards when only the fire door and one exit door is open.

Other full-scale tests have been conducted at the NASA Johnson Space Center (JSC) in a B-737 fuselage section.[7,8]

These tests utilized small fuel pools (0.6 × 0.6 m) ignited inside the cabin under natural and forced ventilation conditions. Interior panel and seating materials exposed to this fire were tested for their fire response characteristics. In addition, the JSC results were utilized for comparison with the predictions of various mathematical models.

Full-scale test programs have also been conducted at the Boeing Commercial Airplane Company and the Douglas Aircraft Company. The Boeing tests[8] emphasized comparison of full-scale results with small-scale tests of materials. The Douglas cabin fire simulator has been utilized for full-scale testing of lavatory configurations[9] and passenger seat materials[10] and for the development of a combined hazard index (CHI)[11] to be used in the evaluation of relative hazards associated with different interior materials.

The results of these test programs have shown, not surprisingly, that it is still difficult to extrapolate standard small-scale test results directly to the full scale. More importantly, it was found that the major factor affecting fire penetration and spread in an aircraft fuselage is the ambient wind condition.[1-3,6,12,13] In the postcrash situation, wind is almost always present and, when the doors are opened, the pressure distribution over the fuselage can result in significant axial velocity components along the length of the fuselage interior. Thus, an externally initiated fire may be blown through an opening and its spread then augmented by the induced flow along the interior of the fuselage.

Obviously, the above described large-scale tests are expensive to conduct. In addition, many complex phenomena take place that make it difficult to elucidate the mechanisms of fire spread on a detailed basis. To do so would require even more extensive and costly instrumentation than is currently employed. Thus, reduced-scale experiments that incorporate some of the essential elements of the full-scale situation are required and have been carried out. Eklund[14,15] has demonstrated the utility of using reduced-scale (1/16-1/4) tests for simulating the postcrash fire situation. In that work, penetration of an external fire into the fuselage was studied. Also, Quintiere et al.[16] have had some success in 1/7-scale simulations of fire flows in corridor geometries similar to an aircraft fuselage interior.

As part of NASA and FAA efforts to study the postcrash fire scenario, a pool fire and flame spread test facility was built at the Jet Propulsion Laboratory (JPL) to study fire dynamics and flame spread under controlled conditions that simulate actual fire situations in a ⅓-scale aircraft interior geometry. The objectives of the present experimental investigation are to study pool fire and crossflow interactions as they relate to aircraft cabin interior fires under postcrash conditions.

System, Instrumentation, and Experiments

The pool fire and flame spread test facility was designed to simulate a fuel fire that has penetrated an opening in an aircraft fuselage and spread across the width of the interior. The cross-sectional dimensions (0.76 m high × 1.52 m wide) are approximately one-third the dimensions of a wide-body transport aircraft interior. The fuel source is Turbojet-A (kerosene) and the ventilating air supply provides air at flow velocities that replicate possible flow conditions under postcrash conditions.[13] These conditions assume that other doors along the fuselage length have been opened for passenger egress. Pressure differences over the fuselage cylinder due to wind then produce[13] an axial ventilation flow along the fuselage. This ventilation flow along the fuselage length is the condition we simulate here. The data presented describe fire dynamics under varying ventilation crossflow conditions.

The experimental system (Fig.1) is composed of four modular, interchangeable sections of welded 3.2 mm thick hot-rolled steel construction. The test section is 3.4 m long and is covered with 2.5 cm thick ceramic fiberboard insulation. Ventilating airflow is provided by a centrifugal blower that supplies a maximum flow of approximately 57 m^3/min (2000 ft^3/min). A damper upstream of the blower inlet controls the flow rate and pitot and static pressure probes immediately upstream of the blower inlet are used to monitor it. After exiting the blower outlet, the flow is turned 180 deg and passes through two layers of 20 mesh screen and 10 cm of honeycomb upstream of the test section. Hot-film anemometer traverses were taken at several locations in the test section under noncombusting conditions to characterize the incident flow. A summary of the results is presented in the Appendix. Nominal velocities in Table 1 were determined from these data at different flow rates. After leaving the test section, the flow exits through a 61 cm diameter exhaust stack (Fig. 1).

The fuel pan is 0.30 × 1.52 m and spans the width of the test section. It thus provides a 0.3 m "channel" fire across the section. It was estimated that this pan width would produce a pool fire flame height approximately equal to the height of the test section under quiescent conditions based on correlations presented by Thomas.[17] The steel pan is double-walled and cooled by water flowing through a 4.8 mm gap between walls. The typical water flow rate during tests is 12-13 liter/min. The pan is mounted flush with the test section and is 5.1 cm deep. A 2.5 cm thick ceramic fiber blanket covers the bottom and acts as a wick. It was found that a fuel soaked wick provides a relatively uniform burning surface and is more safely controlled. Previous data[18,19] show that burning fuel soaked wicks closely replicate the burning characteristics of open liquid-pool fires.

Prior to the start of a test, the fuel is preheated by a 3.2 mm diameter resistance heating element that is placed in a "U" shape on top of the wick along the length of the pan. This provides for rapid ignition over the entire fuel surface at the start of the test. The fuel is ignited by an external pilot flame inserted through a port in the sidewall of the test section. Complete ignition is achieved over the fuel surface in approximately 5 s, after heating at 600 W for 10 min. The fuel pan is supported from one end by a fulcrum and on the other by a rod in turn supported by a load cell. The fuel pan is completely enclosed by an outer cover attached to the bottom of the test section. The load cell support rod extends to the load cell through a silicone-rubber diaphram fitted in the outer cover. The fuel pan support system provided continuous fuel weight loss data during selected tests.

Gas phase and surface temperature data are provided by 60 chromel-alumel (type K) thermocouples located on probes as shown in Fig. 2. Temperature data is recorded sequentially on a 60 channel data logger sampling at 0.5 s per channel. The probes are located along the test section centerline and at selected off-center spanwise locations as needed for each test. Two water-cooled radiometer and calorimeter pairs are mounted in the ceiling along the centerline of the test section (Fig. 2). The sensing elements are of the thin metallic foil type and the radiometers have sapphire windows purged by a nitrogen gas flow. The time constants for the radiometers and calorimeters are 0.5 and 0.3 s, respectively. The calorimeters and radiometers are calibrated using a tungsten filament quartz lamp reference source before and after each test. Heat flux data during the tests are recorded continuously on strip chart recorders.

Six gas sampling probes are sampled sequentially during tests and analyzed for oxygen concentration. One probe was located in the exhaust stack and the remaining five were in the exit plane of the test section (Fig. 2). Each line is sampled for 5 s in sequence and cycling is continuous. The oxygen concentration data are utilized to calculate the energy release rates during the steady period of the tests by oxygen consumption calorimetry.[20] Finally, soot is sampled continuously from the exhaust stack during tests and collected on two glass fiber filters in series.

Twelve viewports are provided for visual/photographic observations upstream of and along the test section (Fig. 2). Five flow direction probes are located 40-50 cm off the test

section centerline and extend 38 cm down from the test section ceiling. The probes (Fig. 3) are 10 cm wide rectangles constructed from 3.2 mm steel rod. Thin 0.01 mm thick Kapton strips are attached loosely at both ends at 2.5 cm intervals along the length of the probe. The strips are spaced at 1.27 cm intervals along the top 5.1 cm adjacent to the ceiling. The flow direction is then indicated by the direction in which the strips are blown or bowed; the direction of the flow is recorded as a function of vertical height by observers during experiments.

In this study of pool fires with crossflow, tests have been conducted for three crossflow velocities in a range that simulates postcrash wind-induced flow (0.24-0.8 m/s). Approximately 4 liters of Turbojet-A (kerosene) fuel is used to saturate the wick. The three crossflow velocities are equivalent to approximately 100, 50, and 25% full flow.

Previous studies of liquid pool fires in crossflow have been directed toward the effects of wind on the geometry of the flame region and the resulting radiation effects.[21-23] Channel fires were studied in calibrated crossflows, either with an essentially unconfined vertical geometry[21] or with a vertical height-to-pool width ratio (H/b) that was much greater[22,23] than the present study. Welker et al.[22,23] looked at $H/b > 12$, while in the present experiment $H/b = 2.5$. Also, Fu's work[21] was carried out by drawing the airflow over the pool fire using a suction duct. Fuel evaporation rates were not measured for channel fires in the Fu study, while results obtained from fuel evaporation rate measurements by Welker et al. were apparently ambiguous. Both studies reported a strong wind effect on visible flame geometry, and Welker determined drag coefficients from a momentum balance. However, only the visible flame geometry was characterized and details of the plume were not reported in detail. In any case, differences in the geometry and flow conditions between the two cited studies and the present one did not allow direct application to the present situation.

Results and Discussion

The results of pool fire-ventilation crossflow experiments obtained in the JPL facility are summarized in Table 1. They include three tests at different crossflow velocities utilizing the cooled fuel pan and one earlier test (A) that used an uncooled pan at full flow.

The total energy release $\dot{Q}$ was calculated by oxygen consumption calorimetry using O_2 depletion measurements in the exhaust stack during the quasisteady period. The available chemical energy $\dot{Q}_a$ was calculated by taking the product of fuel mass evaporation rate and the heat of combustion for Turbojet A (42.78 kJ/g). Using these quantities, combustion "efficiency" η was determined for tests B and C. Energy convected out the exhaust stack $\dot{Q}_s$ was calculated from the temperature in the stack and the measured mass flow rate through the test section. The energy required to evaporate the fuel $\dot{Q}_e$ is the product of fuel evaporation rate and heat of vaporization (291 J/g). For comparison, the heat transferred to the pan cooling water $\dot{Q}_w$ was determined by measuring water flow rate with a rotameter and the temperature rise between pan inlet and outlet. Other quantities shown in Table 1 will be discussed later.

Composite plots of time-varying data for temperature, oxygen concentration in the exhaust stack, fuel mass loss, and heat flux are given in Fig. 4 for the cooled-pan tests (B-D). They show that, in general, after an approximately 30 s transient, a relatively stable period of burning was maintained for an additional 1.5-2 min. Thereafter, burning gradually decreased in intensity. This tendency is believed to be due to

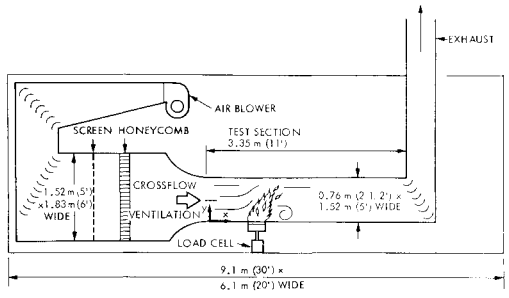

Fig. 1 Experimental system diagram.

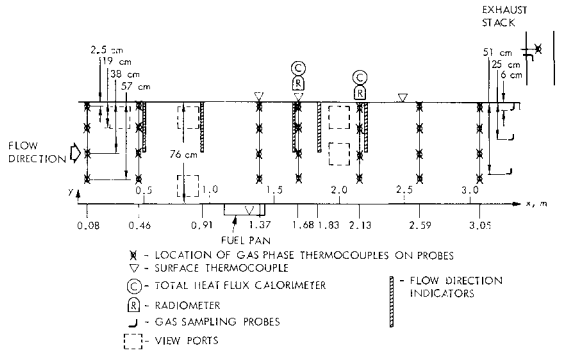

Fig. 2 Instrumentation and measurement locations in the test section.

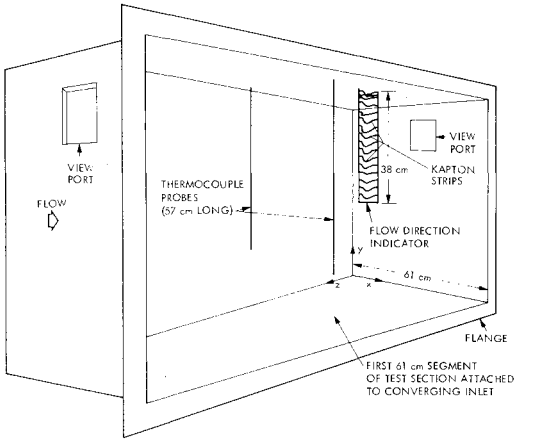

Fig. 3 Flow direction probe and two temperature probes located in the first 0.6 m of the test section.

Table 1 Pool fire-ventilation crossflow test conditions

Test	Flow	$\bar{u}$, m/s	$\dot{Q}$, kW	T_m, K	$\dot{m}_f$, g/s	$\dot{Q}_a$, kW	$\dot{Q}_s$, kW	η, %	$\dot{Q}_w$, kW	$\dot{Q}_e$, kW	$\dot{q}_{r_1}$, W/cm^2	$\dot{q}_{t_1}$, W/cm^2	$\dot{q}_{r_2}$, W/cm^2	$\dot{q}_{t_2}$, W/cm^2	h_1, cm	h_s, cm	ρ_s, g/cm^3 $\times 10^6$	T_a, K
A	Full[a]	0.80	215	862	NA[b]	NA[b]	140	NA[b]	NA[b]	NA[b]	NA[b]	NA[b]	NA[b]	NA[b]	NA[b]	NA[b]	NA[b]	289
B	Full	0.80	140	720	3.6	154	110	91	2.5	1.05	1.0[c]	1.0[c]	0.5[c]	0.7[c]	14[d]	20	0.2	285
C	½	0.43	125	880	4.1	175	70	71	4.4	1.19	1.0[c]	1.2[c]	0.5[c]	0.6[c]	25	50	NA[b]	292
D	¼	0.24	125	910	NA[b]	NA[b]	58	NA[b]	3.5	NA[b]	0.7[c,e]	0.7[c,e]	0.3[c]	0.6[c]	27	76	0.3	286

[a]Uncooled fuel pan. [b]Not available. [c]Estimated mean value after steady period established. [d]For test B: $h_2 = 19$ cm, $h_3 = 6.4$ cm, $h_4 = 4.1$ cm, $h_5 = 0$. [e]Highest peaks at 2.0-2.5 W/cm^2.

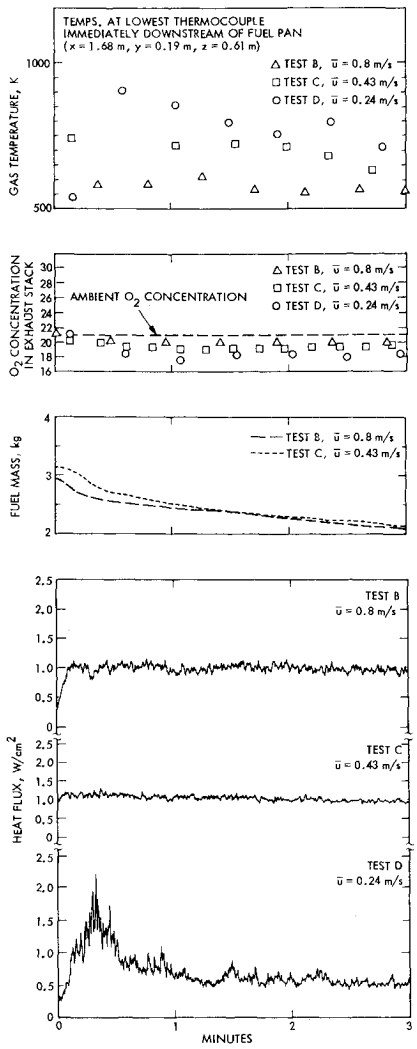

Fig. 4 Composite plots of characteristic temperature, oxygen concentration in the exhaust stack, fuel mass loss, and total heat flux ($\dot{q}_{t_1}$) vs time for tests B, C, and D.

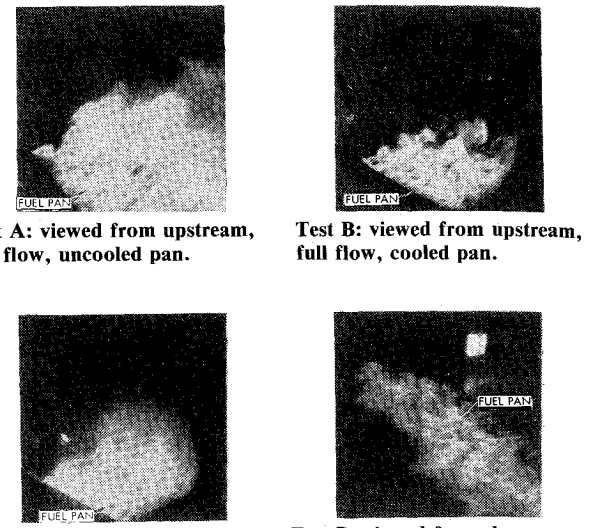

Test A: viewed from upstream, full flow, uncooled pan.

Test B: viewed from upstream, full flow, cooled pan.

Test D: viewed from upstream, ¼ flow, cooled pan.

Test B: viewed from downstream, full flow, cooled pan.

Fig. 5 Flame geometries viewed from up- and downstream of the fuel pan (note: scales of B and D are the same; view of test A is from a closer distance than of B and D).

the effect of the wick gradually being depleted of fuel with a resulting reduced capillary action effect.

The photographs in Fig. 5 show the flame geometries for three of the tests viewed from upstream of the fuel pan and one view from downstream at full flow (bottom right). They show that at full flow the visible, luminous portion of the flame tip is blown downstream approximately 0.5 m with a flame height peak at 30-40 cm above the floor of the test section. This strong crossflow effect was similar for the test at ½ full flow, although it appeared to the observers that the flame tip was blown over further than in the full-flow tests. For test D at ¼ flow, the photograph shows an initial flattening of the fire over the pan, but then a more vertical flame profile just downstream of the pan.

Figure 6 shows temperature isotherms for each of the four tests listed in Table 1. These data are averages of temperatures over the 1.5-2 min steady period of each test and averaged spatially at each point in the spanwise direction. Minimal variation in temperatures in the spanwise direction was observed (Fig. 7), thus indicating that the fire and flow environment is two-dimensional in the mean. In all tests, peak temperatures were measured at the lowest thermocouple located just downstream of the fuel pan ($x = 1.68$ m). Instantaneous maximum (peak) temperatures T_m for all tests are listed in Table 1. Other general features of the temperature field (Fig. 6) indicate a cooler gas region above the flame zone, associated primarily with the crossflow blowing effect, and a higher gas temperature region near the ceiling that also extended far upstream of the fire. For the full-flow tests, the gas temperatures were less for the test with the cooled fuel pan (test B) compared to the uncooled fuel pan (test A) results. The effect of lower crossflow velocities for the cooled fuel pan results was to increase the gas temperatures, as indicated by comparing tests B-D in Fig. 6. Further discussion of the associated gas dynamics follows subsequently.

The temperature measurements were made with unshielded, beaded junction thermocouples. Such measurements are subject to radiation errors, depending upon gas temperature, gas-phase absorption characteristics, and proximity to the fire.[24] Estimates of radiation errors for the present experimental conditions show that the temperatures are overestimated by less than 30 K in regions just upstream of the fire (within 0.2 m) and less than 10 K in regions far upstream (greater than 1 m). Errors in hot, sooty regions up and downstream of the fire appear to be minimal.[24]

The results show that the heat release rate was highest for test A at full flow using the uncooled fuel pan (Table 1). For the same flow rate with the cooled fuel pan (test B), the heat release rate was reduced by 35%. Heat release rates during the tests at reduced ventilation rates were even lower. Thus, the relatively small amount of heat removed in cooling the pan has a major effect on the fuel burning rate. This is presumably due to the fact that the fuel pan cooling rate $\dot{Q}_w$ is relatively large compared to the energy $\dot{Q}_e$ required to evaporate the fuel. That is, for a given rate of energy feedback from the fire to the fuel pan, less energy is available to evaporate the fuel.

The lower energy release rates at lower crossflow velocities are likely due to reduced, less efficient mixing at the lower velocities in the two-dimensional geometry. Note that the calculated combustion efficiency at the full flow rate is significantly greater than at the ½ flow rate. On the other hand, the fuel evaporation rate was higher at the ½ flow of test C when compared to the full flow of test B. This may be due to the fact that as the flow velocity decreased, the average temperatures in the test section increased (Fig. 6). This could result in more rapid heating and evaporation at the pool surface, although the combustion was still relatively inefficient. Clearly, however, combustion efficiency, heat release, and heat feedback to the fuel pool are complex processes that are very sensitive to the mixing of the crossflow with the fire and

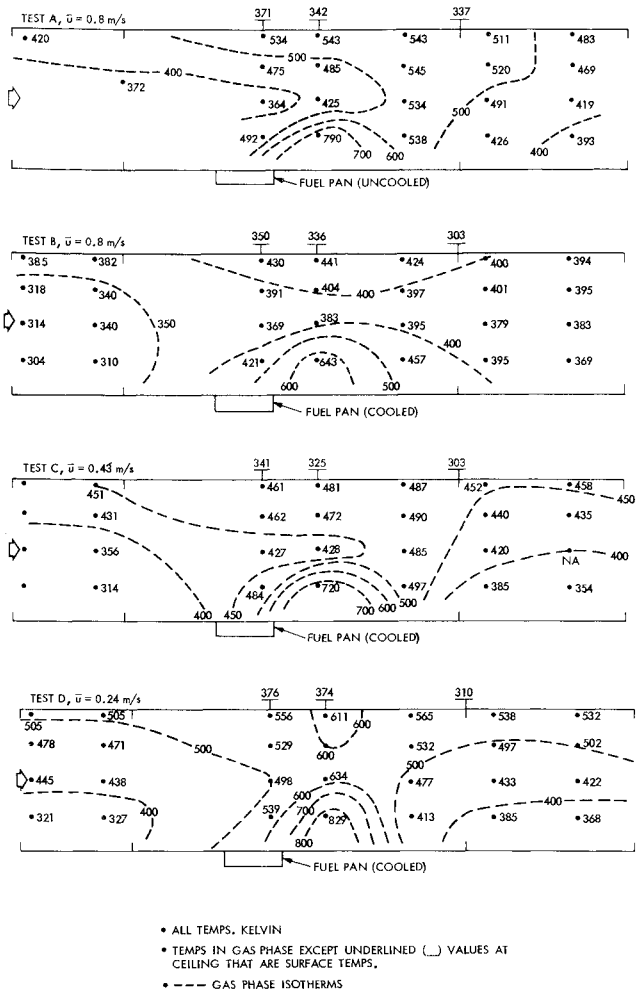

Fig. 6 Average temperatures and isotherms in the test section during tests A-D.

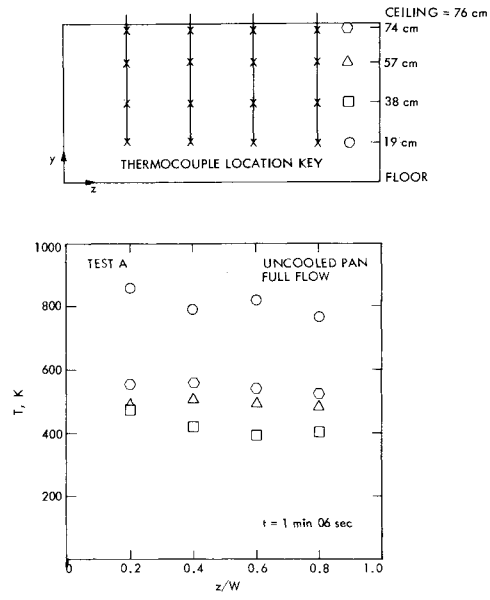

Fig. 7 Spanwise temperature variation in the test section during test A, $x = 1.68$ m, 0.25 m downstream of the edge of the fuel pan (viewed looking downstream).

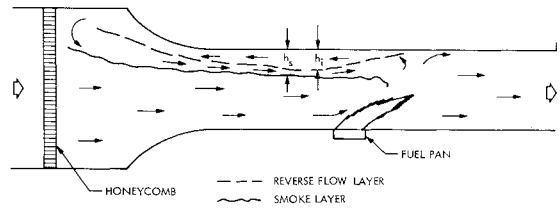

Fig. 8 Flowfield and smoke layer characteristics in test B (full flow, $\bar{u} = 0.8$ m/s, cooled fuel pan).

plume. In fact, combustion efficiencies can be very low, even though the airflow is usually an order of magnitude in excess of stoichiometry based on measured fuel evaporation rates.

For all tests, a strong reverse flow ceiling jet of heated gas was observed well upstream of the fire. This result is (by the temperature measurements) indicated in Fig. 6 and was confirmed by the flow direction probes. In test B (Fig. 8), the reverse-flow region extended from 50-60 cm downstream of the edge of the fuel pan ($x \simeq 2$ m), where the plume stagnation region is located, back into the converging section upstream of the test section inlet. Little or no smoke was detected upstream of the honeycomb and thus the reverse flow was turned and recirculated at that point. Recirculation of the smoke back into the main flow resulted in the smoke layer being lower than the reverse-flow region (Fig. 8 and Table 1).

The existence of the reverse-flow region is somewhat surprising in view of the observed effect of crossflow on the *visible* flame geometry. While the flame is blown over significantly, heated gas still reaches the ceiling with enough momentum to establish the reverse-flow situation. However, this phenomenon was observed about 30 years ago in studies of mine fires and a preliminary analysis was carried out by Thomas.[25] He defined a fire-crossflow parameter as the ratio of the buoyancy head ($g\beta H\theta$) to the velocity head of the ventilation flow ($\bar{u}^2/2$). By using the approximate energy balance $\dot{Q} \simeq \rho_g \bar{u} c A \theta$, this ratio $\mathcal{F}$ can be written as

$$\mathcal{F} = \frac{2gH\dot{Q}}{\rho_g c T_s A \bar{u}^3} \qquad (1)$$

Thomas[25] found that when $\mathcal{F} \gtrsim 5$, then a reverse flow ceiling jet will occur. Values of $\mathcal{F}$ were equal to nine or greater for all of the tests described herein; thus, the reversed flow region is predicted according to this criterion and we have observed it in all of these tests.

Subsequently, experimental and analytical work by the U.S. Bureau of Mines[26,27] led to the definition of a similar nondimensional grouping. In a 0.3×0.3 m tunnel where all four walls were burning wood,[26] they found $\mathcal{F} \cong 4.5$ during incipient reverse flow. The analytical treatment[27] uses a two-dimensional, two-layer (ceiling jet and plume) model to calculate the characteristics and penetration distance of the reverse-flow region, assuming the fire to be on the floor. The model[27] is similar to the geometry of the present experiments and the predicted features of the flow are qualitatively similar to our experimental observations. However, since the reverse flow region extends back into the converging section for all of the tests reported here, a detailed comparison with the Bureau of Mines model is not possible. Future experiments are planned with an extended upstream test section.

It is interesting to note that even though the present experiments were two-dimensional in the mean, the transport of hot combustion products to the ceiling occurs. That is, since streamlines do not cross one another, it would not be possible for gas in the buoyant plume to reach the ceiling when crossflow ventilation exists in two dimensions. However, these flows are clearly turbulent and turbulence is inherently three-dimensional. Presumably, the transport of hot combustion products to the ceiling is due to the existence of relatively large-scale turbulent structures and this is supported by the

three-dimensional structures visible in Fig. 5. In any case, the type of fire and flow situation occurring in our experiments has been observed in large- and small-scale situations[25,26] with varying geometries, including three-dimensional effects. Thus, we believe these data are also indicative of the case when the fire does not extend across the width of the test section and, in fact, we observed this in subsequent tests.[28] Furthermore, these new data add to the detailed knowledge of the structure of this type of fire and flow configuration. Such data are needed to aid in the development of models describing fire in crossflow situations.

The effect of reducing crossflow velocity was to increase the depth h_1 of the reverse flow region (Table 1). For test C at ½ flow, the reverse-flow layer almost doubled in depth, while the plume became slightly more vertical in orientation. However, near the fuel pan, the visible flame was blown over at least as much as in the full-flow case. Note also that the reverse-flow layer has the effect of reducing the effective cross-sectional area of the incoming ventilating crossflow. In turn, this increases the flow velocity incident on the pool fire for the same mass flow rate of ventilating air. For test C at ½-flow velocity, it is estimated that the effect would be to increase the crossflow velocity by a factor of at least 1.5 based on the thickness of the ceiling layer and by invoking continuity.

The geometry of the fire and plume at ¼-flow rate (test D) was more vertically oriented than in previous tests. This is evident in the photograph in Fig. 5 and in Fig. 6d. The reverse-flow region h_1 was only slightly deeper than in the test at ½ flow (test C), while the smoke layer h_s extended to the floor of the test section (Table 1). Apparently, a limit has been reached whereby no further significant reverse-flow layer depth increase will occur. That is, the tendency to deepen the ceiling layer is balanced by the combination of forced ventilation and the flow entrainment process at the base of the fire. The smoke layer has extended to the floor at ¼ flow due to more smoke being transported and introduced into the ventilating flow at lower levels upstream of the test section.

Other data show that, for the conditions studied, heat fluxes at the ceiling are usually 1 W/cm^2 or less, 70-80% of this being radiative (Table 1). In the case of the ¼-flow tests, heat fluxes peaked initially at 2.0-2.5 W/cm^2 and decreased steadily thereafter (Fig. 4). Maximum heat fluxes were recorded at the position ($x=1.68$ m) in the ceiling closest to the fuel pan, followed by a drop in levels 0.5 m further downstream ($x=2.13$ m) as indicated in Table 1. Also, the heat flux data (Fig. 4) indicated a pulsation frequency of 1-2 Hz during the steady period of most tests and this was confirmed by slow motion replay of video tape recordings of the fire. Oxygen concentrations varied somewhat over the exit plane as shown in Fig. 9, where oxygen depletion did not vary significantly from the exhaust stack measurments. The data in Fig. 9 are averages for the 1.5-2 min steady period of each test. Finally, soot concentration in the exhaust stack was estimated from the total sampled mass of soot in tests B and D. The results (Table 1) indicated higher soot densities ρ_s at the lower ventilation rate. Further analysis of relative soot production rates will require accurate measurement of the fuel weight loss and soot production under all test conditions.

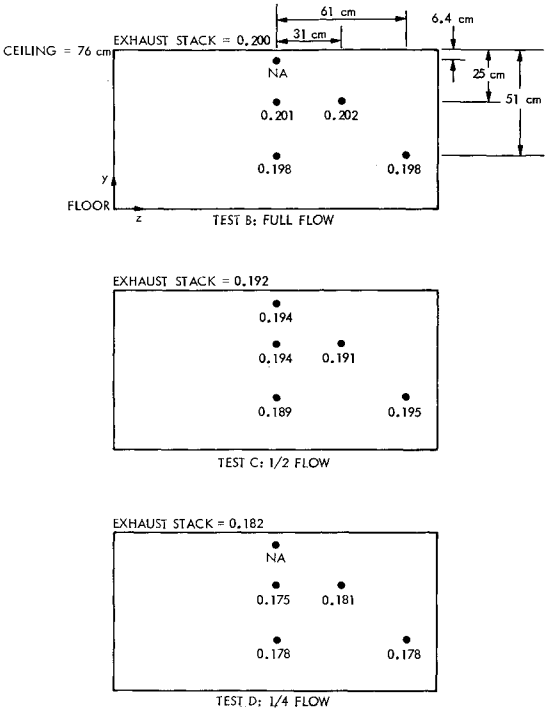

Fig. 9 Average oxygen concentrations in the exit plane of the test section during tests B, C, and D (viewed looking downstream).

Conclusions

A pool fire and flame spread test facility has been built at the Jet Propulsion Laboratory to study pool fire dynamics in a ventilating crossflow and flame spread across aircraft interior materials. The geometry is one-third the scale of a wide-body transport aircraft interior with a "channel" pool fire extending the width of the test section. The first series of pool fire ventilation crossflow experiments have been conducted with the following findings:

1) The temperature and flowfield in the test section was observed to be essentially two-dimensional in the mean. The fuel pan/wick system provided a steady period of burning of 1.5-2 min during each test.

2) Pool fire heat release rates were strongly affected by water cooling the fuel pan. When the pan cooling rate was of the same order as the heat required to evaporate the fuel, heat release was reduced 35%.

3) Peak temperatures measured were 862 K in a 215 kW fire in an uncooled pan at the full-flow rate ($\bar{u}=0.8$ m/s) and 910 K in a 125 kW fire in a water-cooled pan at the ¼-flow rate ($\bar{u}=0.24$ m/s).

4) For the experimental conditions studied, the pool fires were characterized by pulsations at approximately 1-2 Hz.

5) Heat release rates tended to decrease with crossflow velocity, possibly due to a decrease in the efficiency of mixing. Combustion efficiency also decreased with the ventilation rate.

6) The visible flame geometry was blown over significantly under all test conditions except the lowest crossflow velocity. However, a reverse-flow ceiling jet of hot gas still was formed and extended well upstream of the fire. The thickness of the reverse-flow layer deepened as crossflow velocity decreased until an apparent limit was reached near ¼ full flow (0.24 m/s).

7) The existence of the reverse-flow ceiling jet is consistent with earlier studies of mine fires and a criteria that predicts conditions for the onset of reverse flow.

The observed interaction of the ventilation flow with the fire and plume has several implications. First, smoke and toxic gases may spread in both directions within a long ventilated enclosure. This spread may occur in the upstream direction against a significant crossflow velocity (in this case for wind-induced flow through a postcrash aircraft fuselage). Also, the upstream smoke layer in turning to flow in the downstream direction extended to the floor of the test section upstream of the fire at the lowest ventilation rate, thus contaminating the fresh air region above the floor that was present in the higher ventilation rate tests. These observations are also important to the evaluation of in-flight aircraft fire hazards, since apparently only a physical barrier would be effective in stopping the spread of smoke and toxic gases from a strong fire source.

Second, the reverse flow ceiling jet may enhance flame spread along the ceiling against the ventilation flow. Evidence for this occurring has been observed in mine fires.

Finally, there is a range of crossflow velocities for which the effective cross-sectional area of the incoming flow is reduced by the reverse-flow ceiling layer such that the blowing effect of the visible, most luminous part of the flame is enhanced. This might further accelerate flame spread along the floor in the downstream direction.

Appendix: Test Section Flow Characterization

The ventilating flow in the pool fire and flame spread facility test section was characterized by hot-film anemometry. Floor-to-ceiling traverses were carried out at several streamwise and spanwise locations in the test section upstream of the fuel pan. The sensor was mounted on an 80 cm probe and traversed from top to bottom by an electrical motor drive at approximately 10-15 cm/min. The hot-film probe was a standard straight probe (TSI model 1210-10) with a 25 μm diameter wire. The anemometer is a TSI model 1053B with a model 1051 monitor and power supply. The upper frequency response of this system is approximately 10 kHz. Calibration of the probe for the flow range of interest was carried out before and after all runs.

Typical velocity profiles at three locations in the test section and at three flow rates are given in Fig. A1. Figure A1a shows the data taken near the test section inlet on the centerline. Velocities varied by 10-15% over the section height at full and ½ flows and turbulent fluctuations were less than 5%. However, a significant velocity deficit is evident in the lower half of the test section at ¼ flow and large turbulent fluctuations are indicated. Clearly at the low flow rate, the flow had not recovered from the 180 deg turn through the sharp right-angle bends downstream of the blower outlet. Significant turbulence was apparently generated in the section at the blower outlet expansion and in the sharp turns, particularly at the low flow rate.

Further downstream on the centerline (Fig. A1b), the velocity profiles were more uniform along the vertical axis and turbulence levels were lower. This location is two-thirds of the distance from test section inlet to fuel pan and it is reasonable to expect that the velocity profiles were further improved at the fuel pan. Thus, the incident velocities at the fuel pan are fairly represented by an average velocity at the centerline.

Variation of the velocity profiles in the spanwise direction may be deduced from Fig. A1c, which shows the vertical profiles at $x=0.81$ m (same as in Fig. A1b) and $z=0.38$ m ($z/W=0.25$). The velocity profiles and turbulence levels at full and ½ flow were essentially the same as on the centerline. At ¼ flow, the mean velocity profile was nearly the same as at the test section centerline; however, the turbulence levels were higher. These data thus show that mean velocities and turbulence levels were relatively uniform over the entire cross section. The exception was at ¼ flow, where the turbulence levels increased significantly near the sidewalls. The nominal crossflow velocities tabulated for reference purposes in Table 1 were determined from the measured mean velocity profiles just upstream of the fuel pan on the test section centerline (i.e., Fig. A1b).

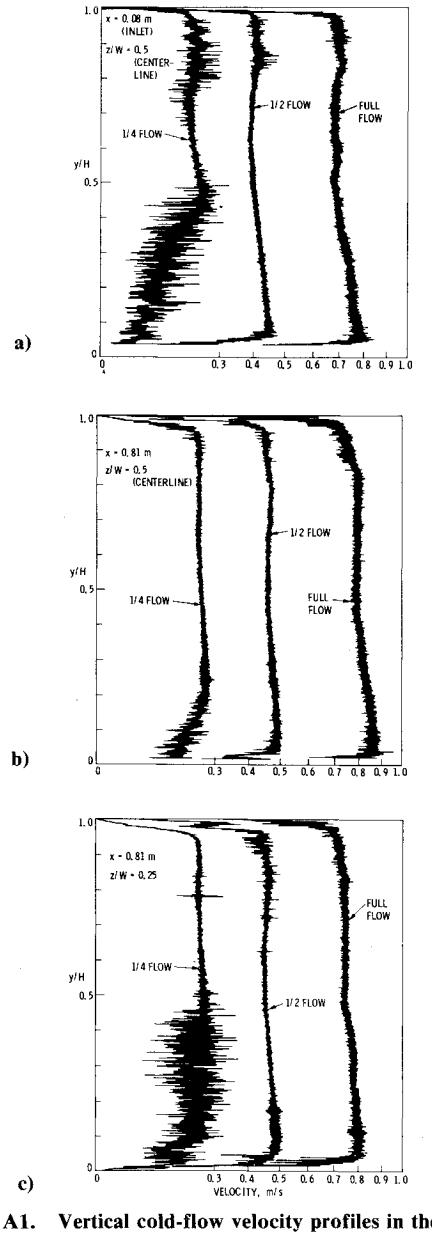

Fig. A1. Vertical cold-flow velocity profiles in the test section.

Acknowledgments

This work presents the results of research carried out by the Jet Propulsion Laboratory, California Institute of Technology, under contract with the National Aeronautics and Space Administration. The work was supported by the Transport Aircraft Aviation Safety Program, Office of Aeronautics and Space Technology (OAST) of NASA. Mr. A. R. Tobiason was the program manager at NASA. The authors also thank Messrs. D. C. Schneider and J. J. Godley for their contributions in fabrication, assembly, and instrumentation of the test facility. Assisting in the conduct of the experiments were Messrs. Schneider and Godley and Drs. Y. I. Cho and S. P. Parthasarathy. Drs. Cho and Parthasarathy conducted the hot-film anemometer traverses to characterize the flow. Finally, we gratefully acknowledge the support and suggestions of Dr. Thor Eklund at the FAA Technical Center during the development of the JPL facility.

References

[1]Hill, R. G., Johnson, G. R., and Sarkos, C. P., "Post-crash Fuel Fire Hazard Measurements in a Wide-Body Aircraft Cabin" U.S. Department of Transportation, Federal Aviation Administration, Atlantic City, NJ, Rept. FAA-NA-79-42, Dec. 1979.

[2]Eklund, T. I. and Sarkos, C. P., "The Thermal Impact of External Pool Fires on Aircraft Fuselages," *Journal of Fire and Flammability*, Vol. 11, July 1980, pp. 231-240.

[3]Hill, R. G. and Sarkos, C. P., "Post-Crash Fuel Fire Hazard Measurements in a Wide-Body Aircraft Cabin," *Journal of Fire and Flammability*, Vol. 12, April 1980, pp. 151-162.

[4]Sarkos, C. P., Hill, R. G., and Howell, W. D., "The Development and Application of a Full-Scale Wide-Body Test Article to Study the Behavior of Interior Materials During a Post Crash Fuel Fire," *Journal of Fire and Flammability*, Vol. 13, July 1982, pp. 172-202.

[5]Sarkos, C. P., Spurgeon, J. C., and Nicholas, E. B., "Laboratory Fire Testing of Cabin Materials Used in Commercial Aircraft," *Journal of Aircraft,* Vol. 16, Feb. 1979, pp. 78-89.

[6]Quintiere, J. G. and Tanaka, T., "Some Analysis of the FAA Post Crash Aircraft Fire Scenario," *Fire Technology,* Vol. 19, No. 2, May 1983, pp. 77-89.

[7]Kuminecz, J. F. and Bricker, R. W., "Full-Scale Flammability Test Data for Validation of Aircraft Fire Mathematical Models," NASA TM 58244, Feb. 1982.

[8]Tustin, E. A., "Development of Fire Test Methods for Airplane Interior Materials," NASA CR-14568, Oct. 1978.

[9]Schutter, K. J. and Klinck, D. M., "Cabin Fire Simulator Lavatory Tests," Final Report for NASA Contract NAS9-15591, May 1980.

[10]Schutter, K. J., Gaume, J. G., and Duskin, F. E., "Testing of Aircraft Passenger Seat Cushion Materials-Full Scale," Final Report for NASA Contract NAS9-16062, Feb. 1981.

[11]Spieth, H. H., Gaume, J. G., Luoto, R. E., and Klinck, D. M., "A Combined Hazard Index Fire Test Methodology for Aircraft Cabin Materials," U.S. Department of Transportation, Federal Aviation Administration, Atlantic City, NJ, Rept. DOT/FAA/CT-82/36, April 1982.

[12]Eklund, T. I., "Preliminary Evaluation of the Effects of Wind and Door Openings on Hazards Development Within a Model Fuselage From an External Pool Fire," U. S. Department of Transportation, Federal Aviation Administration, Atlantic City, NJ, Letter Rept. NA-79-1-LR, Feb. 1979.

[13]Stuart, J. W., "Fuselage Ventilation Due to Wind Flow About a Postcrash Aircraft," Jet Propulsion Laboratory, California Institute of Technology, Pasadena, JPL Pub 80-36, June 1980.

[14]Eklund, T. I., "Pool Fire Radiation Through a Door in a Simulated Aircraft Fuselage," U.S. Department of Transportation, Federal Aviation Administration, Atlantic City, NJ, Rept. FAA-RD-78-135, Dec. 1978.

[15]Eklund, T. I., and Wright, J. A., "Fuel Fire Hazard Penetration into a Model Fuselage as a Function of Circumferential Door Location and Fuel Bed Height," U.S. Department of Transportation, Federal Aviation Administration, Atlantic City, NJ, Rept. FAA-NA-80-9, May 1980.

[16]Quintiere, J., McCaffrey, B. J., and Kashiwagi, T., "A Scaling Study of a Corridor Subject to a Room Fire," *Combustion Science and Technology,* Vol. 18, 1978, pp. 1-19.

[17]Thomas, P. H., "The Size of Flames From Natural Fires," *Ninth Symposium (International) on Combustion,* Academic Press, New York, 1963, pp. 844-859.

[18]Wood, B. D., Blackshear, P. L., and Eckert, E. R. G., "Mass Fire Model: An Experimental Study of the Heat Transfer to Liquid Fuel Burning from a Sand-filled Pan Burner," *Combustion Science and Technology,* Vol. 4, 1971, pp. 113-129.

[19]Blackshear, P. L. Jr. and Murty, K. A., "Some Effects of Size, Orientation, and Fuel Molecular Weight on the Burning of Fuel-Soaked Wicks," *11th Symposium (International) on Combustion,* The Combustion Institute, Pittsburg, PA, 1967, pp. 545-552.

[20]Krause, R. F., Jr. and Gann, R. G., "Rate of Heat Release Measurements Using Oxygen Consumption," *Journal of Fire and Flammability,* Vol. 12, 1980, pp. 117-130.

[21]Fu, T. T., "Aviation Fuel Fire Behavior Study," Aircraft (Ground) Fire Suppression and Rescue System Program Office, Wright-Patterson Air Force Base, OH, Tech. Rept. AGFSRS 72-2, Feb. 1972.

[22]Welker, J. R., Pipkin, O. A., and Sliepcevich, C. M., "The Effect of Wind on Flames," *Fire Technology,* Vol. 1, May 1965, pp. 122-129.

[23]Welker, J. R. and Sliepcevich, C. M., "Bending of Wind Blown Flames from Liquid Pools," *Fire Technology,* Vol. 2, May 1966, pp. 127-135.

[24]Newman, J. S. and Croce, P. A., "A Simple Aspirated Thermocouple for Use in Fires," *Journal of Fire and Flammability,* Vol. 10, Oct. 1979, pp. 326-336.

[25]Thomas, P. H., "The Movement of Buoyant Fluid Against a Stream and the Venting of Underground Fires," Fire Research Station, Boreham Wood, England, Fire Research Note 351, 1958.

[26]Lee, C. K., Chaiken, R. F., and Singer, J. M., "Interaction Between Duct Fires and Ventilation Flow: An Experimental Study," *Combustion Science and Technology,* Vol. 20, 1979, pp. 59-72.

[27]Hwang, C. C., Chaiken, R. F., Singer, J. M. and Chi, D.N.H., "Reverse Stratified Flow in Duct Fires: A Two-Dimensional Approach," *16th Symposium (International) on Combustion,* The Combustion Institute, Pittsburgh, PA, 1977, pp. 1385-1395.

[28]Bankston, C. P. and Back, L. H., "Measurements of the Flow and Heat Transfer Characteristics for Pool Fires in a Simulated Aircraft Cabin Interior with Ventilation," paper presented at Fall Technical Meeting, Eastern Section, Combustion Institute, Dec. 1984.